OCCAM

OXFORD CENTRE FOR COLLABORATIVE APPLIED MATHEMATICS

Indentation of ellipsoidal and cylindrical elastic shells

by

Dominic Vella
Amin Ajdari
Ashkan Vaziri
Arezki Boudaoud

OCCAM Preprint Number 12/68

Indentation of ellipsoidal and cylindrical elastic shells

Dominic Vella[1], Amin Ajdari[2], Ashkan Vaziri[2] and Arezki Boudaoud[3]
[1] *OCCAM, Mathematical Institute, University of Oxford, 24-29 St Giles', Oxford, OX1 3LB, UK*
[2] *Department of Mechanical and Industrial Engineering, Northeastern University, Boston, MA, 02115, USA*
[3] *Laboratoire Reproduction et Développement des Plantes & Laboratoire Joliot-Curie, INRA, CNRS, ENS, Université de Lyon, 46 Allée d'Italie, F-69364 Lyon Cedex 07, France*

Thin shells are found in nature at scales ranging from viruses to hens' eggs; the stiffness of such shells is essential for their function. We present the results of numerical simulations and theoretical analyses for the indentation of ellipsoidal and cylindrical elastic shells, considering both pressurized and unpressurized shells. We provide a theoretical foundation for the experimental findings of Lazarus *et al.* [*Phys. Rev. Lett.* (submitted)] and for previous work inferring the turgor pressure of bacteria from measurements of their indentation stiffness; we also identify a new regime at large indentation. We show that the indentation stiffness of convex shells is dominated by either the mean or Gaussian curvature of the shell depending on the pressurization and indentation depth. Our results reveal how geometry rules the rigidity of shells.

PACS numbers: 46.32.+x, 46.70.De, 62.20.mq

Everyday experience shows that it is easier to crack an egg on its side than at its tip. This observation has led to demonstrations in children's science programmes, such as the successful landing of a helicopter on an array of eggs [1]. This rigidity is a common feature of other convex elastic shells ranging from viral capsids, plant and fungal cells to the pressure vessels used to store gases. Although this rigidity is known to be geometric in origin (such shells cannot deform without stretching) and conditions on whether a shell is geometrically rigid have been derived [2], this property has not been comprehensively quantified.

A common assay of a shell's rigidity is the measurement of an 'indentation stiffness'. This test can be performed at scales ranging from nanoscale viruses [3] through microscopic polymer capsules [4] to macroscopic beach balls [5]. Theoretical predictions for the indentation stiffness of spherical shells are well known [6–8] and have recently been extended to incorporate the effect of an internal pressure [5]. The predictions of these models have been borne out by experiments on microscopic capsules and membranes [4, 9–11], and macroscopic balls [5, 8, 12, 13]. The theoretical study of cylinders under indentation is limited to some specific examples, namely cytoskeletal microtubules [14] and bacterial cells [15], while at a macroscopic scale thin sheets bent into cylindrical shapes have been studied [16, 17].

Although most previous theoretical work has addressed the idealized cases of spherical or cylindrical shells, an understanding of the behavior of ellipsoidal shells would often be more appropriate, particularly in the case of yeast cells [18, 19] or bacteria [15]. Numerical explorations of more general shapes and mechanical properties include shells of arbitrary convexity [20] as well as axisymmetric membrane shells in a nonlinear elastic framework motivated by seed germination [21]; however, no quantification of the indentation stiffness was provided in these studies. Recently, a comprehensive experimental study of the stiffness of moderately elongated ellipsoids [22] has been presented, leading the authors to propose heuristic formulae for the stiffness and call for more theoretical work. In this Letter we use theoretical arguments and numerical simulations to provide a comprehensive study of the geometrical rigidity of convex thin shells. Our model experiment is the indentation of a shell at a single point (see fig. 1). By considering shells with and without an applied pressure difference we demonstrate that an important component of the geometrical rigidity disappears with the application of such a pressure difference.

The important feature of a shell are its radii of curvature, and so we lose little generality by considering an ellipsoidal elastic shell with axes a, b and c and centered at the origin (see fig. 1). The surface of the ellipsoid is thus given in Cartesian coordinates by

$$\frac{x^2}{a^2} + \frac{y^2}{b^2} + \frac{z^2}{c^2} = 1 \tag{1}$$

The shell has Young's modulus E, Poisson ratio ν and thickness t, yielding a bending stiffness $B = Et^3/[12(1-\nu^2)]$. For simplicity, we shall assume here that indentation occurs at the point $(0, 0, c)$ (see fig. 1). The question of principal interest in this Letter is the relationship between the indentation force applied, F, and the indentation displacement, δ. To answer this question, we shall develop a model based on the theory of shallow shells [23, 24]. In this limit, it is the surface shape close to the point of indentation that matters, and so we write

$$z \approx c - x^2/2R_x - y^2/2R_y \tag{2}$$

where $R_x = a^2/c$ and $R_y = b^2/c$ are the principal radii of curvature. Therefore, although our theoretical results will be couched in terms of the indentation of an ellipsoid,

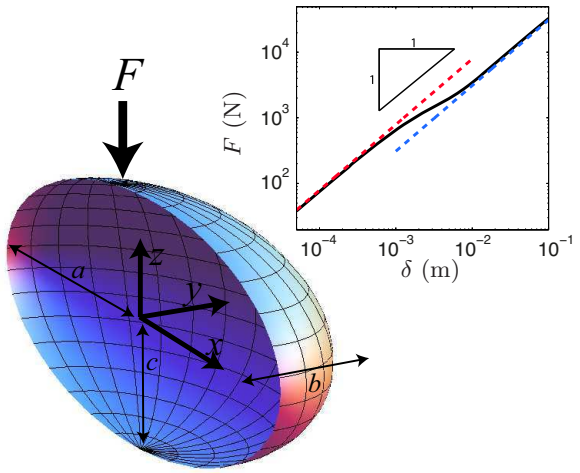

FIG. 1. (Color online) The indentation of ellipsoidal shells. Main figure: Cut away view of an ellipsoid centered on the origin and subjected to a point force at $(0, 0, c)$. Inset: Numerically determined force–displacement curve for a spherical shell with $a = b = c = 1$ m, $E = 70$ GPa, $\nu = 0.3$, $t = 2$ mm subject to an internal pressure $p = 10^5$ Pa. The two linear regimes considered here are shown as dashed lines.

they apply more generally to shapes with differing radii of curvature (though we require the Gauss curvature $\kappa_G = R_x R_y > 0$).

The midline of the shell is displaced by an amount $w(x, y)$ from its undeformed state by a given loading. This deformation is determined by coupling the displacement and loading to the components of the stress within the shell, which may be written in terms of the Airy stress function ϕ as $\sigma_{xx} = \partial^2_{yy}\phi$, $\sigma_{yy} = \partial^2_{xx}\phi$ and $\sigma_{xy} = -\partial^2_{xy}\phi$. If the shell is subject to an internal pressure p and the application of a point force F then the nonlinear equations of shallow shell theory may be written [24]

$$B\nabla^4 w + \nabla_k^2\phi - [\phi, w] = p - \frac{F}{2\pi}\frac{\delta(r)}{r} \tag{3}$$

and

$$\frac{1}{Et}\nabla^4\phi - \nabla_k^2 w = -\frac{1}{2}[w, w]. \tag{4}$$

where

$$[f, g] \equiv \frac{\partial^2 f}{\partial x^2}\frac{\partial^2 g}{\partial y^2} - 2\frac{\partial^2 f}{\partial x \partial y}\frac{\partial^2 g}{\partial x \partial y} + \frac{\partial^2 f}{\partial y^2}\frac{\partial^2 g}{\partial x^2} \tag{5}$$

and

$$\nabla_k^2 = \frac{1}{R_x}\frac{\partial^2}{\partial x^2} + \frac{1}{R_y}\frac{\partial^2}{\partial y^2} \tag{6}$$

is the Vlasov operator [24]. Note that Eq. (3) expresses the normal force balance on the shell, with the point forcing represented by a Dirac δ function, and Eq. (4) representing the compatibility of strains. To complement the theoretical study of equations (3)-(4), numerical simulations were performed using the commercial finite element package ABAQUS. For these simulations material properties $E = 70$ GPa and $\nu = 0.3$ were assumed; other details are similar to the spherical case reported previously [5] but relaxing the assumption of axisymmetry.

The equations (3)-(4) have previously been studied in detail for the case of a spherical shell with $a = b = c$, i.e. $R_x = R_y = R$ [5]. This analysis showed the presence of two regimes in the force–displacement curve (see inset of fig. 1). For displacements smaller than the shell thickness, $\delta \ll t$, the indentation force $F = k_1^{(s)}\delta$ where

$$k_1^{(s)} = 4\pi\frac{B}{\ell_b^2}\frac{(\tau^2 - 1)^{1/2}}{\operatorname{arctanh}(1 - \tau^{-2})^{1/2}}, \tag{7}$$

$$\ell_b = \left(\frac{BR^2}{Et}\right)^{1/4}, \quad \tau = \frac{1}{4}\frac{pR^2}{(EtB)^{1/2}}. \tag{8}$$

The length scale ℓ_b represents the horizontal distance over which vertical deformations decay without an internal pressure, while τ gives a dimensionless measure of the stress within the shell due to this pressure. For vertical displacements $\delta \gg t$ and strong pressurization, $\tau \gg 1$, a boundary layer analysis of eqns (3)-(4) gave [5] that $F = k_2^{(s)}\delta$ where

$$k_2^{(s)} = \pi p R. \tag{9}$$

The experiments of Lazarus *et al.* [22] concern the small deformation behavior (i.e. k_1) for ellipsoidal shells with two out of the three lengths a, b and c set equal (i.e. ellipsoids of revolution). They considered two cases: 'indentation at a pole' and 'indentation along a meridian'. The case of 'indentation at a pole' may be obtained within our formulation by setting $a = b$. In this case we have that $R_x = R_y$: the shell is locally spherical and the indentation response is described by the spherical case recapped above with the radius of curvature $R = a^2/c$. The remainder of this Letter is concerned with indentation at points where the two principal radii of curvature are different, $R_x \neq R_y$. To simplify our analysis, we begin by considering the case of ellipsoidal shells with zero internal pressure.

In the limit of unpressurized shells, $p = 0$, Eqns (3)-(4) simplify considerably upon linearizing and splitting the Vlasov operator according to

$$\nabla_k^2 = \kappa_M\nabla^2 + \Delta\kappa\left(\frac{\partial^2}{\partial x^2} - \frac{\partial^2}{\partial y^2}\right). \tag{10}$$

Here $\kappa_M \equiv (R_x^{-1} + R_y^{-1})/2$ is the mean curvature and $\Delta\kappa \equiv (R_x^{-1} - R_y^{-1})/2$ is a measure of the asphericity of the shell. Eqns (3)-(4) can be non-dimensionalized by letting $X = x/\ell_b, Y = y/\ell_b, W = w/\ell_b$ etc., with ℓ_b

redefined from (8) with $R = \kappa_M^{-1}$, $\mathcal{F} = F \times \ell_b/B$ and $\Phi = \phi \times \ell_b \kappa_M / B$. We find that

$$\nabla^4 W + \nabla^2 \Phi + \frac{\Delta\kappa}{\kappa_M}\left(\frac{\partial^2 \Phi}{\partial X^2} - \frac{\partial^2 \Phi}{\partial Y^2}\right) = -\frac{\mathcal{F}}{2\pi}\frac{\delta(R)}{R} \quad (11)$$

$$\nabla^4 \Phi - \nabla^2 W - \frac{\Delta\kappa}{\kappa_M}\left(\frac{\partial^2 W}{\partial X^2} - \frac{\partial^2 W}{\partial Y^2}\right) = 0 \quad (12)$$

It is clear from (11)-(12) that in the limit of $\epsilon \equiv \Delta\kappa/\kappa_M \ll 1$ we should recover the results previously found for a spherical shell. This observation suggests positing series for Φ, W and $\mathcal{F}$ in powers of ϵ. The solution of the resulting problem can be found analytically for the terms up to and including the ϵ^2 term [25]. This analysis shows that $F = k_1 \delta$ with

$$k_1 = (1 - \epsilon^2/2 + ...) k_1^{(s)}(\tau = 0), \quad (13)$$

which agrees well with the results of simulations shown in fig. 2 for $\epsilon \ll 1$, as expected. However, we note that for larger values of ϵ the expression

$$k_1 = (1 - \epsilon^2)^{1/2} k_1^{(s)}(\tau = 0), \quad (14)$$

provides an even more satisfactory fit. Furthermore, in the limit $\epsilon \to \pm 1$ (a cylindrical shell) it is known [14] that $k_1 \sim Et^{5/2}/R^{3/2} \sim k_1^{(s)}(t/R)^{1/2} \ll k_1^{(s)}$ for $t/R \ll 1$, consistent with the vanishing of $k_1/k_1^{(s)}$ as $\epsilon \to \pm 1$. However, we are unable to rationalize this observation from shallow shell theory; we leave this as a result that may be of interest to future researchers and shall return to its geometrical interpretation later.

We now consider the case of pressurized shells for which the base state prior to the beginning of indentation is no longer simply a uniform displacement independent of x and y. At the point $(0, 0, c)$ a pressurized ellipsoid of revolution has an anisotropic stress state [26] in which

$$\sigma_{xx}^0 = \tfrac{1}{2} p R_y, \quad \sigma_{yy}^0 = \tfrac{1}{2} p R_y \left(2 - \frac{R_y}{R_x}\right). \quad (15)$$

Because of these two complications, we present here only the results of numerical simulations. Nevertheless we use some of the ideas developed in the unpressurized case to guide our analysis. In particular, we note that it is natural to use $R = \kappa_M^{-1}$ as the characteristic radius of curvature and that shallow shell theory leads to a term of the form $\sigma_{ij}\partial_{ij} w$. Therefore it is natural to use the isotropic part of the base state stress, $\sigma_M = (\sigma_{xx}^0 + \sigma_{yy}^0)/2 \neq p/2\kappa_M$, in the definition of the dimensionless pressure τ. We therefore write that

$$\tau = \frac{1}{2}\frac{\sigma_M}{(EtB\kappa_M^2)^{1/2}} = \frac{p}{4\,(EtB)^{1/2}\,\kappa_M^2} f(\kappa_G/\kappa_M^2) \quad (16)$$

where $f(\xi) = \left[2 + \left(\sqrt{1-\xi} - 1\right)/\xi\right] / \left(\sqrt{1-\xi} + 1\right)$. Note that $\sigma_M = 3p/8\kappa_M$ for a circular cylinder ($\kappa_G = 0$) and $\sigma_M = p/2\kappa_M$ for a sphere ($\kappa_G = \kappa_M^2$). Using this definition of τ and $R = \kappa_M^{-1}$ we plot the results of our numerical simulations in Fig. 3. We see that as τ increases beyond $O(1)$ the results converge to the corresponding $\tau \gg 1$ result for a spherical shell, namely

$$k_1 \simeq \frac{4\pi B}{\ell_b^2}\frac{\tau}{\log 2\tau}. \quad (17)$$

This result generalizes the formula proposed by Lazarus *et al.* [22] for moderately elongated ellipsoids. It can also be compared with previous work aiming at inferring bacterial turgor pressure from measurement of k_1 by Arnoldi *et al.* [15]. Their study built an *ab initio* model for the bacterial wall and for rubber ballons inflated by internal pressure. They assumed that the shape was cylindrical and, furthermore, that the stress within the shell was isotropic and equal to the mean value, σ_M in our notation. Our systematic investigation of the indentation of pressurized elastic shells using numerical simulations in ABAQUS supports their assumption that σ_M is the appropriate stress scale. However, our theory yields the correct prefactor $1/\log 2\tau$ and is valid for any dimensionless pressure, as well as for ellipsoidal shells which are more realistic models of bacterial cells.

We now consider larger indentation depths ($\delta \gg t$) and the limit of high pressure ($\tau \gg 1$). As for small displacements, we sought to rescale the numerically-determined force-displacement curves onto the theoretical results obtained for a spherical shell in these limits [5]. This analysis reveals that the best collapse of the numerical data

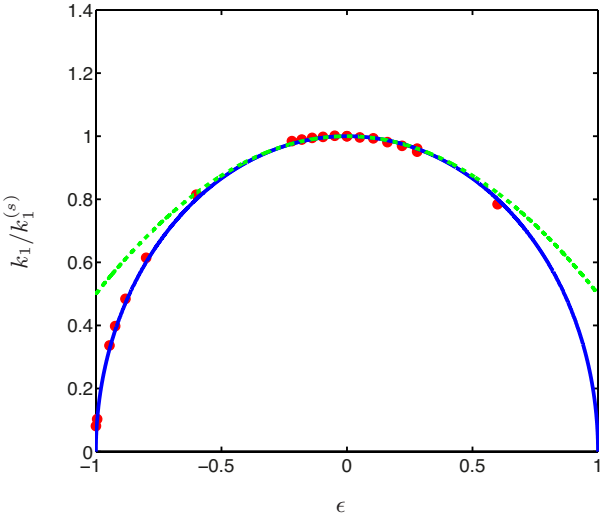

FIG. 2. (Color online) The stiffness of unpressurized ellipsoidal shells, k_1, compared to the stiffness of a sphere with the same mean curvature κ_M, $k_1^{(s)}$, plotted as a function of the asphericity parameter $\epsilon = (R_y - R_x)/(R_x + R_y)$. The asymptotic expression (13) (dashed curve) agrees well with numerical results for $\epsilon \ll 1$. However, the fit (14) (solid curve) gives a good account even for $\epsilon = O(1)$. Numerical data were obtained in simulations with $t = 5$ mm and $b = c = 1$ m.

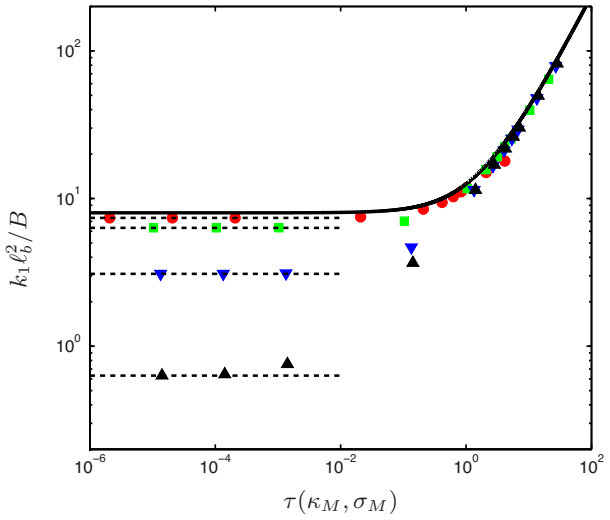

FIG. 3. (Color online) The small-deformation stiffness of pressurized ellipsoidal shells, k_1, as a function of the dimensionless pressure τ, given in (16). Results are shown for ellipsoids with $t = 0.005$, $b = c = 1$ and $a = 0.75, \epsilon \approx 0.28$ (●), $a = 2, \epsilon \approx -0.6$ (■) and $a = 5, \epsilon \approx -0.92$ (▼) as well as for a horizontal cylinder with radius $1, \epsilon = -1$ (▲), which corresponds to $a = \infty$. Here the length scale ℓ_b is determined using the mean curvature κ_M and $\tau = \tau(\kappa_M, \sigma_M)$. The analytic prediction for the corresponding sphere, (7), is shown by the solid curve. Dashed horizontal lines show the corresponding value of k_1 for $p = 0$ (see fig. 2).

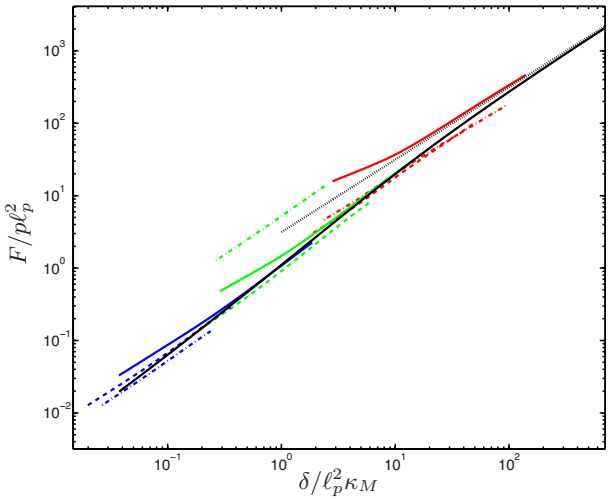

FIG. 4. (Color online) Force-displacement curves at large displacements. The results of ABAQUS simulations are shown for shells with $a = 5$ m, $\kappa_G/\kappa_M^2 = 0.148$ (dashed curves), $a = 2.5$ m, $\kappa_G/\kappa_M^2 = 0.476$ (dash-dotted curves) and $a = 1$ m, $\kappa_G/\kappa_M^2 = 1$ (solid curves). The simulated shells have thickness $t = 2$ mm, $b = c = 1$ m and a variety of internal pressures: $p = 10^5$ Pa (red), $p = 10^6$ Pa (green) and $p = 10^7$ Pa (blue). Here κ_M^{-1} is used as the radius of curvature in ℓ_p. Numerical (solid black curve) and asymptotic (dotted line) results for a spherical membrane shell [5] are also shown.

is obtained by using the typical radius $R = \kappa_M^{-1}$ with the lengthscale $\ell_p = (p/Et)^{1/2}\kappa_M^{-3/2}$, which emerges from a balance between in-plane stretching and the geometric stretching caused by the internal pressure [5, 27]. This result suggests that large indentations combined with high pressure leads to an almost isotropic tension within the shell — the situation resembles the indentation of a sphere.

In this Letter we have studied the effects of asphericity on the indentation response of ellipsoidal and cylindrical elastic shells. In the absence of an internal pressurization, we found that the indentation force required to produce a vertical displacement δ is $F = k_1\delta$ where

$$k_1 = 8\,(BEt\kappa_G)^{1/2}\,. \tag{18}$$

We note that in this result it is the Gaussian curvature, $\kappa_G = (R_xR_y)^{-1}$, rather than the mean curvature κ_M that provides the relevant length scale. Indeed Gaussian curvature is associated with in-plane stretching, and so it is natural that it appears in the quantification of geometric rigiditiy. In the case of highly pressurized shells $\tau \gg 1$, however, we found that

$$F = \begin{cases} \frac{\pi f(\kappa_G/\kappa_M^2)}{\log 2\tau} p\kappa_M^{-1}\delta, & \delta \ll t \\ \pi p\kappa_M^{-1}\delta, & \delta \gg t \end{cases} \tag{19}$$

In this regime, the stiffness can be accounted for simply by using results from the spherical case together with the mean curvature and mean base stress. This conclusion provides strong theoretical support for an assumption made in previous analyses [15, 22] and provides the necessary theoretical background for the measurement of turgor pressure in systems better modelled using ellipsoidal, rather than spherical, shells. Finally, we note that the internal pressure in cells may be modified by altering the osmolarity of the external medium [5, 19]. Therefore, the combination of unpressurized and pressurized stiffnesses presented here may enable the measurement of both shell wall modulus and turgor pressure in a wide range of practical problems.

This publication is based on work supported in part by Award No. KUK-C1-013-04, made by King Abdullah University of Science and Technology (KAUST) (D.V.). A.A. and A.V. are thankful for the support of NSF CMMI Grant No. 1149750. A.B. was supported by ANR-10-BLAN-1516. During the completion of this work, we benefited from discussions with A. Lazarus and P. Reis about their experiments on a similar system [22].

[1] Richard Hammond's Blast Lab, Episode 1, 2012.
[2] B. Audoly and Y. Pomeau, *Elasticity and Geometry* (Oxford University Press, 2010).
[3] W. H. Roos, R. Bruinsma, and G. J. L. Wuite, Nature Phys. **6**, 733 (2010).
[4] V. D. Gordon, X.Chen, J. W. Hutchinson, A. R. Bausch,

M. Marquez, and D. A. Weitz, J. Am. Chem. Soc. **126**, 14117 (2004).
[5] D. Vella, A. Ajdari, A. Vaziri, and A. Boudaoud, J. R. Soc. Interface **9**, 448 (2012).
[6] E. Reissner, J. Math. Phys. **25**, 80 (1947).
[7] E. Reissner, J. Math. Phys. **25**, 279 (1947).
[8] A. V. Pogorelov, *Bending of Surfaces and Stability of Shells* (AMS Bookstore, Providence, RI, 1988).
[9] E. Helfer, S. Harlepp, L. Bourdieu, J. Robert, F. C. MacKintosh, and D. Chatenay, Phys. Rev. Lett. **87**, 088103 (2001).
[10] C. I. Zoldesi, I. L. Ivanovska, C. Quilliet, G. J. L. Wuite, and A. Imhof, Phys. Rev. E **78**, 051401 (2008).
[11] R. Bernal, C. Tassius, F. Melo, and J. C. Geminard, Eur Phys J E **34** (2011).
[12] J. R. Fitch, Int. J. Solids Structures **4**, 421 (1968).
[13] L. Pauchard and S. Rica, Phil. Mag. B **78**, 225 (1998).
[14] P. J. de Pablo, I. A. T. Schaap, F. C. MacKintosh, and C. F. Schmidt, Phys. Rev. Lett. **91** (2003).
[15] M. Arnoldi, M. Fritz, E. Baüerlein, M. Radmacher, E. Sackmann, and A. Boulbitch, Phys. Rev. E **62**, 1034 (2000).
[16] A. Boudaoud, P. Patrício, Y. Couder, and M. Ben Amar, Nature **407**, 718 (2000).
[17] M. Das, A. Vaziri, A. Kudrolli, and L. Mahadevan, Phys. Rev. Lett. **98**, 014301 (2007).
[18] A. E. Smith, Z. Zhang, C. R. Thomas, K. E. Moxham, and A. P. J. Middelberg, Proc. Natl. Acad. Sci. USA **97**, 9871 (2000).
[19] J. Arfsten, S. Leupold, C. Bradtmöller, I. Kampen, and A. Kwade, Colloids Surf. B: Biointerfaces **79**, 284 (2010).
[20] A. Vaziri and L. Mahadevan, Proc. Natl. Acad. Sci. USA **105**, 7913 (2008).
[21] S. P. Pearce, J. R. King, and M. J. Holdsworth, Int. J. N. Lin. Mech. **46**, 1128 (2011).
[22] A. Lazarus, H. C. B. Florijn, and P. M. Reis, Phys. Rev. Lett.(2012).
[23] C. R. Calladine, *Theory of Shell Structures* (Cambridge University Press, Cambridge, UK, 1983).
[24] E. Ventsel and T. Krauthammer, *Thin Plates and Shells: Theory, Analysis and Applications* (Marcel Dekker, New York, 2001).
[25] See supplementary information (EPAPS No. . xxxx).
[26] S. P. Timoshenko and S. Woinowsky-Krieger, *Theory of Plates and Shells* (McGraw-Hill, Singapore, 1959).
[27] D. Vella, A. Ajdari, A. Vaziri, and A. Boudaoud, Phys. Rev. Lett. **107**, 174301 (2011).

RECENT REPORTS

12/45	Stochastic models of intracellular transport	Bressloff Newby
12/46	The effects of noise on binocular rivalry waves: a stochastic neural field model	Webber Bressloff
12/47	An Ensemble Bayesian Filter for State Estimation	Farmer
12/48	Simulation of cell movement through evolving environment: a fictitious domain approach	Séguis Burrage Erban Kay
12/49	The Mathematics of Liquid Crystals: Analysis, Computation and Applications	Majumdar
12/50	Fourier spectral methods for fractional-in-space reaction-diffusion equations	Bueno-Orovio Kay Burrage
12/51	Meniscal tear film fluid dynamics near Marx's line	Zubkov Breward Gaffney
12/52	Validity of the Cauchy-Born rule applied to discrete cellular-scale models of biological tissues	Davit Osborne Byrne Gavaghan Pitt-Francis
12/53	A thin rivulet or ridge subject to a uniform transverse shear stress at its free surface due to an external airflow	Sullivan Paterson Wilson Duffy
12/54	The Stokes boundary layer for a thixotropic or antithixotropic fluid	McArdle Pritchard Wilson
12/55	Thermoviscous Coating and Rimming Flow	Leslie Wilson Duffy
12/56	On the anomalous dynamics of capillary rise in porous media	Shikhmurzaev Sprittles
12/57	Compactly supported radial basis functions: how and why?	Zhu
12/58	Multiscale reaction-diffusion algorithms: pde-assisted Brownian dynamics	Franz Flegg Chapman Erban
12/59	Numerical simulation of shear and the Poynting effects by the finite element method: An application of the generalised empirical inequalities in non-linear elasticity	Mihai Goriely

12/60	From Brownian dynamics to Markov chain: an ion channel example	Chen Erban Chapman
12/61	Three-dimensional coating and rimming flow: a ring of fluid on a rotating horizontal cylinder	Leslie Wilson Duffy
12/62	A two-pressure model for slightly compressible single phase flow in bi-structured porous media	Soulaine Davit Quintard
12/63	Mathematical modelling plant signalling networks	Muraro Byrne King Bennett
12/64	A model for one-dimensional morphoelasticity and its application to fibroblast-populated collagen lattices	Menon Hall McCue McElwain
12/65	Effective order strong stability preserving RungeKutta methods	Hadjimichael Macdonald Ketcheson Verner
12/66	Morphoelastic Rods Part I: A Single Growing Elastic Rod	Moulton Lessinnes Goriely
12/67	Wrinkling in the deflation of elastic bubbles	Aumaitre Knoche Cicuta Vella

Copies of these, and any other OCCAM reports can be obtained from:

Oxford Centre for Collaborative Applied Mathematics
Mathematical Institute
24 - 29 St Giles'
Oxford
OX1 3LB
England
www.maths.ox.ac.uk/occam